

BlabberSeg: Real-Time Embedded Open-Vocabulary Aerial Segmentation

Haechan Mark Bong^{*}, *Student Member, IEEE*, Ricardo de Azambuja^{*†}, *Member, IEEE*,
Giovanni Beltrame^{*}, *Senior Member, IEEE*

Abstract—Real-time aerial image segmentation plays an important role in the environmental perception of Uncrewed Aerial Vehicles (UAVs). We introduce BlabberSeg, an optimized Vision-Language Model built on CLIPSeg for on-board, real-time processing of aerial images by UAVs. BlabberSeg improves the efficiency of CLIPSeg by reusing prompt and model features, reducing computational overhead while achieving real-time open-vocabulary aerial segmentation. We validated BlabberSeg in a safe landing scenario using the Dynamic Open-Vocabulary Enhanced Safe-Landing with Intelligence (DOVESEI) framework, which uses visual servoing and open-vocabulary segmentation. BlabberSeg reduces computational costs significantly, with a speed increase of 927.41% (16.78 Hz) on a NVIDIA Jetson Orin AGX (64GB) compared with the original CLIPSeg (1.81Hz), achieving real-time aerial segmentation with negligible loss in accuracy (2.1% as the ratio of the correctly segmented area with respect to CLIPSeg). BlabberSeg’s source code is open and available online¹.

Index Terms—TinyML, VLM, Aerial Segmentation, Aerial Computing and CIOt

I. INTRODUCTION

UNMANNED Aerial Vehicles (UAV) are gaining prominent attention from industry and academia, especially with studies focusing on Intelligent UAVs [1]. By mounting AI-capable devices onto UAVs, it is possible to enable Cognitive Internet of Things (CioT) [2] on UAVs and perform image processing and segmentation tasks such as object detection and segmentation, which are essential for the safe automation of flight operations.

With the rise of foundation models such as Large Language Models (LLMs) and Vision Language Models (VLMs), there is an exponential growth of interest in using these models to improve the automation of vehicles and machines [3], [4]. In the context of UAVs, Liu et al. [5] and Bong et al. [6] showcased generative AI capabilities on aerial imaging using foundational models. Other research efforts [7], [8] focused on performing specific tasks such as navigation, planning, exploration and object detection using CioT devices equipped with LLMs. Although promising results were demonstrated, they share a common constraint, which is the requirement of a high performance on-board computer. In particular, recent LLMs and VLMs [9]–[11] require massive computing power during training and segmentation. Due to the limited computational

capabilities of CioT devices, most foundation models on CioT devices are not suitable for real-time decision making.

Numerous works attempted to optimize the efficiency of neural network segmentation on CioT devices, using various techniques such as model compression [12], [13], input filtering [14], [15], and reusing [16], [17]. However, they are static acceleration methods, which may lead to significant performance degradation when used with foundation models. Dynamic approaches like early exit strategies [18], [19] can reduce unnecessary computations, but the substantial dimensions and deep layers of foundation models result in heavyweight early-exit heads. Moreover, optimizing computation efficiency through input data processing, including filtering and reusing do not adequately address the persistent challenge of limited memory on edge-based CioT devices.

To mitigate these computational constraints, Yang et al. [20] proposed moving the computation of foundation models to edge infrastructure. However, such approach is not practical on UAVs operating with unstable wireless connections (forests, caves, etc.). Other approaches focus on Tiny Machine Learning (TinyML), a relatively new concept that focuses on building lightweight learning models to accommodate on-device operations. For example, the Machine Learning Compilation (MLC) project [21] uses memory planning and quantization techniques to reduce computation latency, while Wang et al. [22] and Chen et al. [23] focus on reducing the model size. Although their results are promising, they are built for text-dialogue generation, which is not suitable for UAV operations, which are dependent to multi-modal sensors and camera. Knowledge-distillation based models such as DIME-FM [24], FD-CLIP [25], VLKD [26], and Mobile-SAM [27] are capable of compressing multi-modal foundation models to certain extent, but they are still heavyweight and yet to be tested on real-time CioT devices mounted on UAVs.

We propose BlabberSeg, an optimized and extended version of one of the most common VLM segmentation models CLIPSeg [28], which is based on CLIP (Contrastive Language-Image Pretraining). In UAV operations, there are often multiple detection and segmentation tasks to be performed. Using CLIPSeg, prompting with a single target label performs much better than a prompt with all the target labels due to accumulation of noise and disparity in cosine similarity [29]. A prompt per target label is not only computationally expensive, but also not scalable, especially if the target class is not fixed. Aerial images, especially at high altitudes (100m) typically have low resolution [30].

Within these constraints, BlabberSeg increases segmentation

^{*}MISTLab, École Polytechnique Montréal, Montréal, Canada

[†]Currently at Questat.ca (contributed to this work while at MISTLab).

Contact: haechan.bong@polymtl.ca

This work was supported by the National Research Council Canada (NRC).

¹<https://github.com/MISTLab/BlabberSeg>

speed by reusing prompt and image embeddings without losing the overall segmentation accuracy (the ratio of the correctly segmented area over the ground truth (segmentation of the original CLIPSeg)). Reusing of embeddings becomes exponentially more significant with the number of prompts.

To evaluate BlabberSeg, we consider emergency UAV landing as a target application. Many previous systems dealt with automatic UAV safe landing, but they would mostly limit the maximum altitude to under 30m [31]–[35] since higher altitude makes aerial segmentation very difficult, especially when UAVs are moving. We evaluate BlabberSeg using Google Maps [36] using DOVESEI [29], an emergency safe landing system that uses CLIPSeg [28] for aerial safe landing zone (SLZ) detection at an altitude of 100m. We used an NVIDIA Jetson Orin AGX [37] as a testing device throughout our experimentation. BlabberSeg drastically lowers computational costs, delivering a 927.41% increase in speed (16.78 Hz) on an NVIDIA Jetson Orin AGX (64GB) [37] compared to the original CLIPSeg (1.81 Hz). This allows for real-time aerial segmentation while maintaining minimal reductions in accuracy (2.1%) and mean Intersection over Union (mIoU) (9%).

II. MATERIALS AND METHODS

A. Reusing for Efficiency

BlabberSeg enables significant computational efficiency on CLIPSeg by reusing features to achieve data processing suited for CIoT devices. In a UAV context, input images and prompts are similar in content since the environment where the UAV flies at a given time will stay the same. However, VLMs are designed to take different images and prompts every time they are processed and BlabberSeg can mitigate re-computation through reusing, which is well-suited for lightweight UAV operations. In addition, our model allows multiple prompts on a single image to target multi-label segmentation.

1) *Reusing Positional Embeddings*: The conventional approach with image segmentation involves recalculating positional embeddings for every image, a process that can be computationally resource-intensive. In our optimized approach, we pre-compute the rescaling of positional embeddings, fixing it according to the input image size. While the optimal image size for CLIPSeg is 352, our method accommodates smaller sizes, thereby reducing the overall model size and improving the processing speed. More specifically, our model treats the positional encoding as an “image” that maintain the same number of patches (considering a fixed image size relative to patch size). This interpolated positional encoding is calculated once and reused for subsequent incoming images, eliminating the need for repetitive calculations during segmentation. In cases where a new image has a different size, the positional encoding is dynamically adjusted through shrinking or interpolation to align with the pre-computed positional encoding.

2) *Optimization of CLIP Activations*: In the original CLIPSeg model, the CLIP image encoder and its activations are invoked for each prompt, leading to redundant computations for real-time image processing in UAVs. Our optimization addresses this inefficiency by running CLIP activations

only once per image, which notably reduces the computational redundancy. Furthermore, we simplify the computation of CLIP activations to calculate only the necessary components, avoiding inessential computations that yield the same output as CLIP’s entire image encoder. More specifically, we reduced the original 12 layers used in CLIP to 10 layers by always using batch size one and images with a fixed size, the tensor filled with zeros will be always the same and thus they are reused. This streamlined approach enhances the overall efficiency of the CLIPSeg model, ensuring that only essential computations are performed during semantic segmentation.

3) *Pre-computing FiLM*: In the original CLIPSeg, the model could only reuse conditionals, but our optimized version pre-computes Feature-wise Linear Modulation (FiLM) [38] on conditionals within the decoder per prompt, allowing for their efficient reuse. This advancement significantly reduces computational overhead during the segmentation process, enhancing the model’s overall efficiency of CLIPSeg decoder, allowing for segmentation per prompt with reduced computational complexity.

4) *Image Processing*: In order to facilitate pre and post image processing, input images are normalized and output segmentations use softmax. In addition, each segmentation generated per prompt are fused to generate a final segmentation with all prompts for a single image. Then we apply blur to make segmentation smoother, just like the DOVESEI [29] system.

5) *Hardware Acceleration*: Other than reusing, we accelerated our model using TensorRT and ONNX runtime input/output binding, taking advantage of efficient hardware acceleration. In addition, our model integrated OpenCLIP instead of the original CLIP to address precision-related challenges by casting our model with floating-point 16 (FP16). The internal cast to FP32 in CLIP can disrupt compatibility with FP16, making it challenging to operate with different precision. OpenCLIP provides a solution that enables seamless casting of the entire model to FP16, enhancing flexibility without compromising precision. Our model is then converted to two ONNX models (activations and CLIPSeg decoder) which are then converted to TensorRT engines to further accelerate segmentation time.

In summary, BlabberSeg enables the advantage of using multiple prompts per image in the segmentation process, focusing on reusing essential components to save computations in on-device aerial imaging. These optimizations collectively contribute to a more efficient CLIPSeg model, making it adaptable to a broader range of image sizes while maintaining high performance in semantic segmentation tasks. The proposed model offer a balance between computational efficiency and model accuracy, addressing the computational challenges associated with on-device image segmentation in UAVs.

B. Experiment Setup

Our experiments consist of demonstrating how each reused features increase computational efficiency. Our tests are done in a complex UAV context, which is the use-case of urgent safe landing.

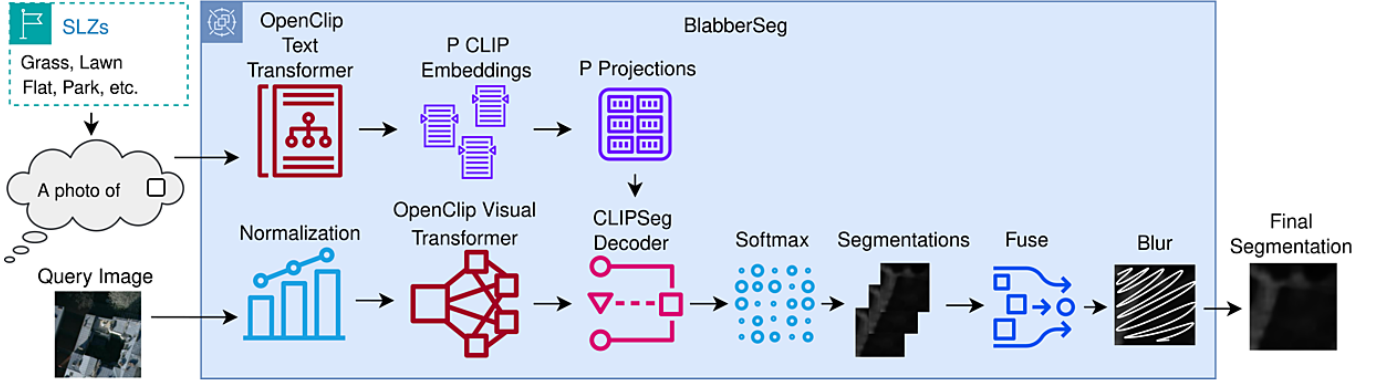


Fig. 1. BlabberSeg Architecture: In this architecture, we harness OpenCLIP Visual Transformer’s capability to cast CLIP into floating-point (FP) 16 and use FP16 converted CLIPSeg Decoder with reused prompt and positional embeddings to accelerate segmentation. P represents the number of prompts, which are the number of words that are selected to describe safe landing zones (e.g. Grass, Lawn, Flat, Park, etc.).

1) *CIoT Device Setup*: In order to facilitate reproducible experiments, all tests are done in NVIDIA Jetson devices [37] and Raspberry Pi 5 [39]. Our main CIoT device for testing was NVIDIA Jetson AGX Orin 64GB [37]. To demonstrate the efficiency of BlabberSeg in less powerful CIoT devices, we also measured performance efficiency using AGX Xavier [37] 64GB, Raspberry Pi 5 [39] (CPU only), and emulated NVIDIA Jetson Orin NX 16GB [37] and NVIDIA Jetson Orin Nano 8GB [37].

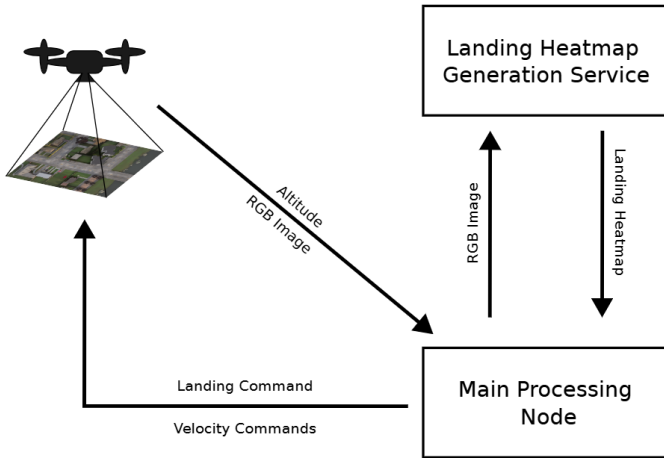


Fig. 2. DOVESEI [29] was implemented in ROS 2 and it is composed of three main blocks: UAV (flight controller, sensors), landing heatmap generation (receives an RGB image and produces a heatmap of the best places to land), and main processing node (orchestrates the data exchange with the UAV, sends velocity commands).

2) *DOVESEI Architecture*: To validate the robustness of our model in a complex and realistic environment, DOVESEI [29] system was used to simulate an urgent UAV safe landing scenario with satellite images of Paris (Google Maps [36]). Using this system, we were able to test our work in high-altitude computing (HAC) and low-altitude computing (LAC) by starting at 100m and descending to 20m. Its system architecture is setup using ROS 2 [40] package and composed of two principal interconnected components: Landing Heatmap Generation Service and Main Processing Node (Fig. 2).

A RGB image and textual prompts serve as inputs to the heatmap generator, which employs BlabberSeg to generate a comprehensive heatmap in a zero-shot manner. This heatmap provides essential insights into optimal landing positions, consistently referred to as “best” within the given image frame context.

The main node assumes high-level control over the entire system and establishes direct connections with the UAV flight controller. Its functionality encompasses three core components: the main state machine, post-processing of raw heatmaps, and dynamic focus.

The state machine governs the dynamic behavior of our system, with its primary states being: **i)** Searching: Coarse search for a landing spot from a safe (collision free) altitude. **ii)** Aiming: Refined search to better align the UAV with a safe landing spot. **iii)** Landing: Descend while checking for dynamic obstacles. **iv)** Waiting: Stop and wait if any obstacles were detected after it started landing. **v)** Climbing: Climb back to the safe altitude if the waiting phase triggered a failure. **vi)** Restarting: Restart the coarse search by moving to a new starting position.

The dynamic focus oversees the degree to which the Raw Heatmap Post-processing module processes the raw heatmap. It selectively “focuses” by applying a binary mask that encompasses specific regions of the input, prioritizing the most crucial areas based on the current system state and its operation.

III. RESULTS AND DISCUSSIONS

In this section, we will refer to TensorRT engine and ONNX runtime input/output binding as TensorRT and Input/Output Binding, respectively.

Our primary objective was to increase CLIPSeg segmentation speed to achieve real-time SLZ detection, ideally optimize throughput to 10Hz. Decrease in segmentation accuracy was expected as an exchange for the gain of segmentation speed. However, we had to ensure that the drop in accuracy is minor in order to be deployed in emergency safe landing applications. Using 500 aerial images [36], we compared the mean segmentation accuracy and Mean Intersection over Union (mIoU)

between the original CLIPSeg (considered as a ground truth) and optimized CLIPSeg models. Our threshold for acceptable mean accuracy and mIoU was set to 90 to ensure that our optimization methods will not hinder segmentation performance. Note that our objective in this experiment was not to measure the segmentation quality, we aim to minimize the change on segmentation results when optimization was applied. The various optimization techniques applied are listed in Table I. We also tried to optimize HF (Hugging Face) version of CLIPSeg, but we realized that their segmentation speeds are much slower than the original CLIPSeg (Table I).

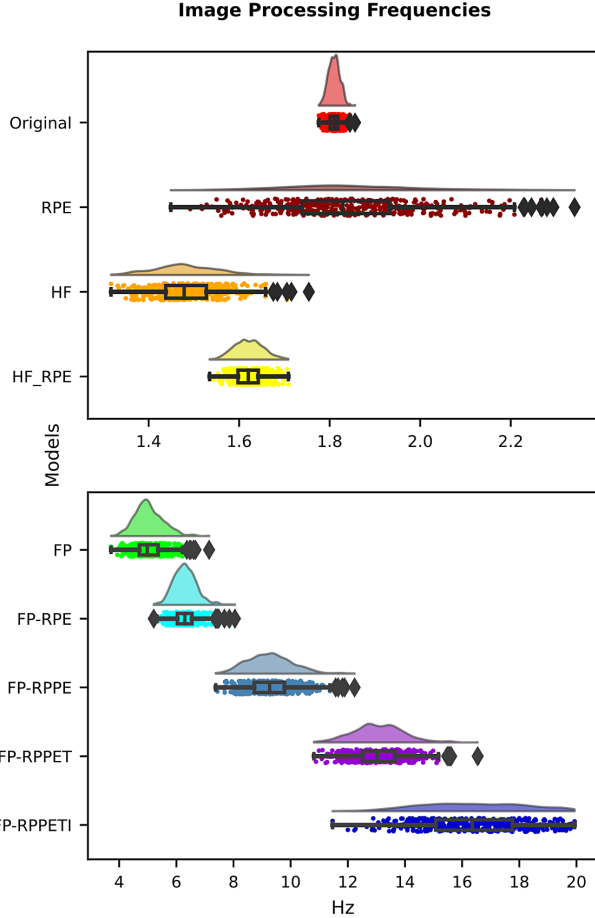


Fig. 3. Increase in Frequency Through Optimization.

Model Legend:
 Original: CLIPSeg (Original)
 FP: CLIPSeg (FP16)
 RPE: CLIPSeg + Reusing Prompt Embeddings
 FP-RPE: CLIPSeg (FP16) + Reusing Prompt Embeddings
 HF: CLIPSeg (Hugging Face)
 HF-RPE: CLIPSeg (Hugging Face) + Reusing Prompt Embeddings
 FP-RPPE: CLIPSeg (FP16) + Reusing Prompt & Positional Embeddings
 FP-RPPET: CLIPSeg (FP16) + Reusing Prompt & Positional Embeddings + TensorRT
 FP-RPPETI: CLIPSeg (FP16) + Reusing Prompt & Positional Embeddings + TensorRT + Input/Output Binding.

A. Computational Efficiency

Through quantization of the model to FP16, we increased the model frequency from 1.81Hz to 4.98Hz (275.13% in-

crease, Fig. 3). Additionally, by reusing prompt and positional embeddings, the model frequency increased to 9.23Hz, which is 509.89% increase compared to the original CLIPSeg. Additional optimization through input/output binding and converting our ONNX model to TensorRT led to an average of 927.41% in improvement. We also analyzed the effect of optimization on image transformation performed before segmentation and noticed that reusing positional embeddings results in significant decrease in image processing time (Fig. 4), contributing to the faster overall frequency.

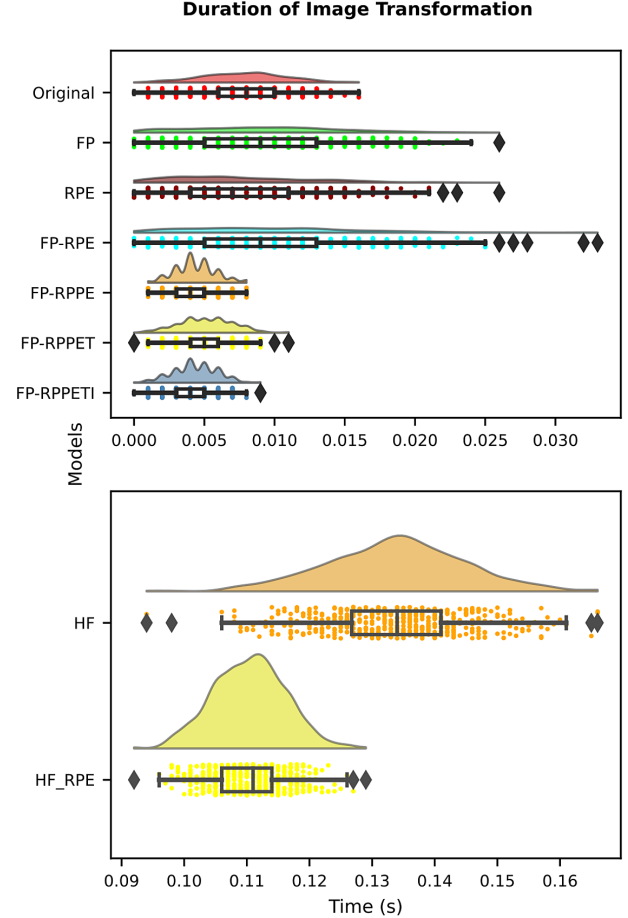


Fig. 4. Duration of Image Transformation before Segmentation.

Using the NVIDIA Jetson's built-in Power GUI, we measured an approximate GPU usage and temperature. Reusing of prompt and positional embedding showed promising results in regards to GPU efficiency. Impressive reduction of GPU utilization and temperature was observed by the reusing architecture as shown in figures 5, 6. Overall, we observed that GPU utilization and temperature dropped almost 10 times and 20°C, respectively, comparing the original CLIPSeg (approximate maximum GPU utilization at 33W and temperature at 68°C) with BlabberSeg (approximate maximum GPU utilization at 3.6W and temperature at 45°C). Note that the GPU measurements are an estimation, but they demonstrate the efficiency of our optimization methods.

GPU Power Consumption Over Time

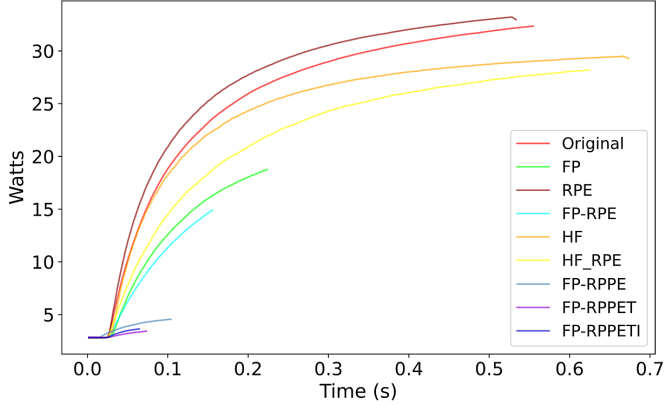


Fig. 5. GPU Usage During Optimization.

Average GPU Temperature Comparison

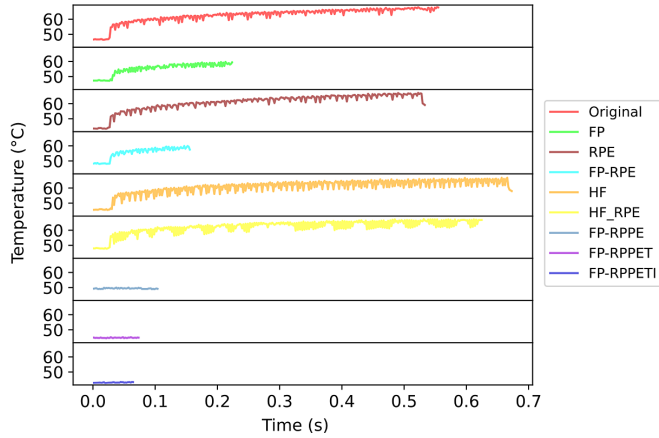


Fig. 6. GPU Temperature Measurement During Optimization.

B. Model Accuracy

We used the original CLIPSeg model accuracy and mIoU as ground truth and compared them with optimized models. Hugging Face models resulted in the same accuracy and mIoU since reusing prompt embeddings does not change anything on the models. As expected, quantization by converting the original CLIPSeg (FP32) to FP16 decreased mean accuracy and mIoU to 99.5 and 99.6, respectively (Table I). For the same reason as reusing prompt embeddings, Input/Output binding did not decrease the accuracy and IoU as expected. Reusing positional embeddings decreased mean accuracy (99.5) and mIoU (97.5) (Table I) slightly, but major drop was from converting the model to TensorRT engine (mean accuracy: 97.9 and mIoU: 91.0) (Table I). As observed in 7, visual difference in segmentation is almost unrecognizable, despite significant gain in efficiency. Overall, NVIDIA Jetson Orin AGX 64GB was able to boost its segmentation frequency from 1.81Hz to 16.78 Hz (Fig. 3) with only marginal differences of 2.1% in accuracy and 9% mIoU (Table I).

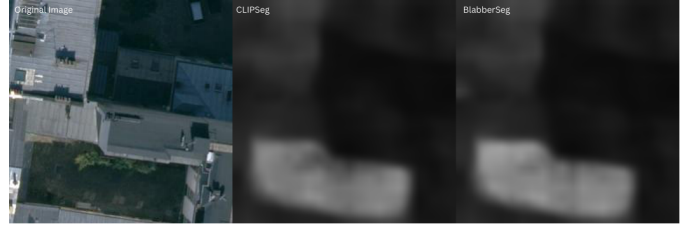


Fig. 7. Difference in Segmentation: Original CLIPSeg (middle) vs BlabberSeg (right).

C. Model Robustness

Aerial images are often in low resolution due to natural condition, rapid motion and high altitude. To address the robustness of the model, additional experiments (100 images) conducted with the images used for our experiments [36], but polluted with random noises. Compared to results generated using images that are not noisy, all metrics performed equally well with noisy images (Fig. 8).

D. Performance on Other IoT Devices

For other IoT devices, we also observed promising increase in speed while keeping relatively high accuracy and mIoU as NVIDIA Jetson Orin AGX 64GB. NVIDIA Jetson Orin NX 16GB was able to increase its speed by 2205.01% and perform segmentation at 14.79Hz, compared to the original CLIPSeg at 1.490Hz (Table II). For NVIDIA Jetson Orin Nano 8G, we achieved 2695.19% increase in speed which is significant and 12.63Hz, compared to 0.47Hz using the original CLIPSeg (Table II). On Jetson AGX Xavier 64G, we observed 2383.23% increase in segmentation speed and 15.18Hz.

We also experimented with Raspberry Pi 5 [39] and measured its performance using only CPU. Due to the CPU's limitation, we measured all models with FP32 and without TensorRT and ONNX runtime. More specifically, CPU architectures are not designed to process FP16 operations or use TensorRT and ONNX enabled models. We observed better performance using the Hugging Face CLIPSeg model (0.04Hz) compared to the original CLIPSeg models (0.02Hz), which was not the case with Jetson devices (Table II). However, their performance were similar after prompt reusing (0.05Hz). The possible reasoning behind the better performance on Hugging Face CLIPSeg model might be related to how it processes the prompts more efficiently using CPU compared to the original CLIPSeg, which might be more efficient in processing the prompts using GPU. Overall, BlabberSeg was able to boost its performance up to 0.17Hz per image segmentation, which is an increase of 715.54% compared to the original CLIPSeg (0.02Hz).

TABLE I
QUANTITATIVE RESULTS OF COMPARISON AMONG ORIGINAL CLIPSEG AND OPTIMIZED CLIPSEG MODELS FOR NVIDIA JETSON ORIN AGX 64G.

Device	Models	Mean Segmentation Duration (s)	Mean Accuracy (%)	mIoU
NVIDIA Jetson Orin AGX 64G	Original	0.553±0.004	100.0 (ground truth)	100.0 (ground truth)
	FP	0.201±0.019	99.5±0.29	99.6±0.36
	HF	0.677±0.032	100.0 (ground truth)	100.0 (ground truth)
	HF-RPE	0.617±0.012	100.0 (ground truth)	100.0 (ground truth)
	RPE	0.547±0.044	100.0 (ground truth)	100.0 (ground truth)
	FP-RPE	0.159±0.010	99.5±0.29	99.6±0.36
	FP-RPPE	0.108±0.009	99.5±0.01	97.7±1.49
	FP-RPPET	0.077±0.006	97.9±1.27	91.0±8.40
	FP-RPPETI	0.060±0.009	97.9±1.27	91.0±8.40

TABLE II
QUANTITATIVE RESULTS OF COMPARISON AMONG ORIGINAL CLIPSEG AND OPTIMIZED CLIPSEG MODELS FOR OTHER NVIDIA JETSON DEVICES

Device	Models	Mean Segmentation Duration (s)	Increase in Speed (%)	Hz
NVIDIA Jetson Orin NX 16G (Emulated)	Original	1.490±0.067	100.0 (ground truth)	0.67±0.0301
	FP	0.420±0.023	354.7±4.31	2.38±0.1296
	HF	1.537±0.040	97.0±0.62	0.65±0.0185
	HF-RPE	1.469±0.0474	101.5±4.27	0.68±0.1285
	RPE	1.364±0.035	109.2±0.55	0.73±0.0166
	FP-RPE	0.378±0.018	394.5±0.73	2.65±0.0220
	FP-RPPE	0.118±0.008	1258.2±18.95	8.44±0.5705
	FP-RPPET	0.094±0.009	1592.6±35.17	10.69±1.0588
	FP-RPPETI	0.068±0.007	2205.0±53.72	14.79±1.6174
NVIDIA Jetson Orin Nano 8G (Emulated)	Original	2.135±0.033	100.0 (ground truth)	0.47±0.0072
	FP	0.594±0.023	359.2±8.91	1.68±0.0643
	HF	2.184±0.017	97.7±2.35	0.46±0.0170
	HF-RPE	2.105±0.016	101.4±8.00	0.48±0.0577
	RPE	2.044±0.071	104.4±0.50	0.49±0.0036
	FP-RPE	0.553±0.018	386.2±0.50	1.81±0.0036
	FP-RPPE	0.150±0.009	1424.7±57.81	6.67±0.4171
	FP-RPPET	0.099±0.007	2147.0±97.29	10.06±0.7019
	FP-RPPETI	0.079±0.008	2695.2±166.29	12.63±1.1997
NVIDIA Jetson AGX Xavier 64G	Original	1.570 ±0.078	100.0 (ground truth)	0.64± 0.0317
	FP	0.419±0.048	374.6±8.72	2.39±0.2767
	HF	1.615±0.051	97.2±0.16	0.62±0.0050
	HF-RPE	1.550±0.040	101.3±3.79	0.65±0.1204
	RPE	1.417±0.010	110.8±0.61	0.71±0.0194
	FP-RPE	0.356±0.015	441.1±0.52	2.81±0.0166
	FP-RPPE	0.112±0.021	1404.4±55.58	8.94±1.7636
	FP-RPPET	0.076±0.003	2055.5±13.63	13.09±0.4326
	FP-RPPETI	0.066±0.008	2383.2±59.78	15.18±1.8970
Raspberry Pi 5	Original	42.973±1.536	100.0 (ground truth)	0.02±0.0008
	HF	27.641±0.888	155.5±0.49	0.04±0.0004
	HF-RPE	21.154±0.255	203.2±1.40	0.05±0.0012
	RPE	21.770±0.193	197.4±0.68	0.05±0.00006
	RPPE	6.096±0.966	715.5±33.03	0.17±0.0275

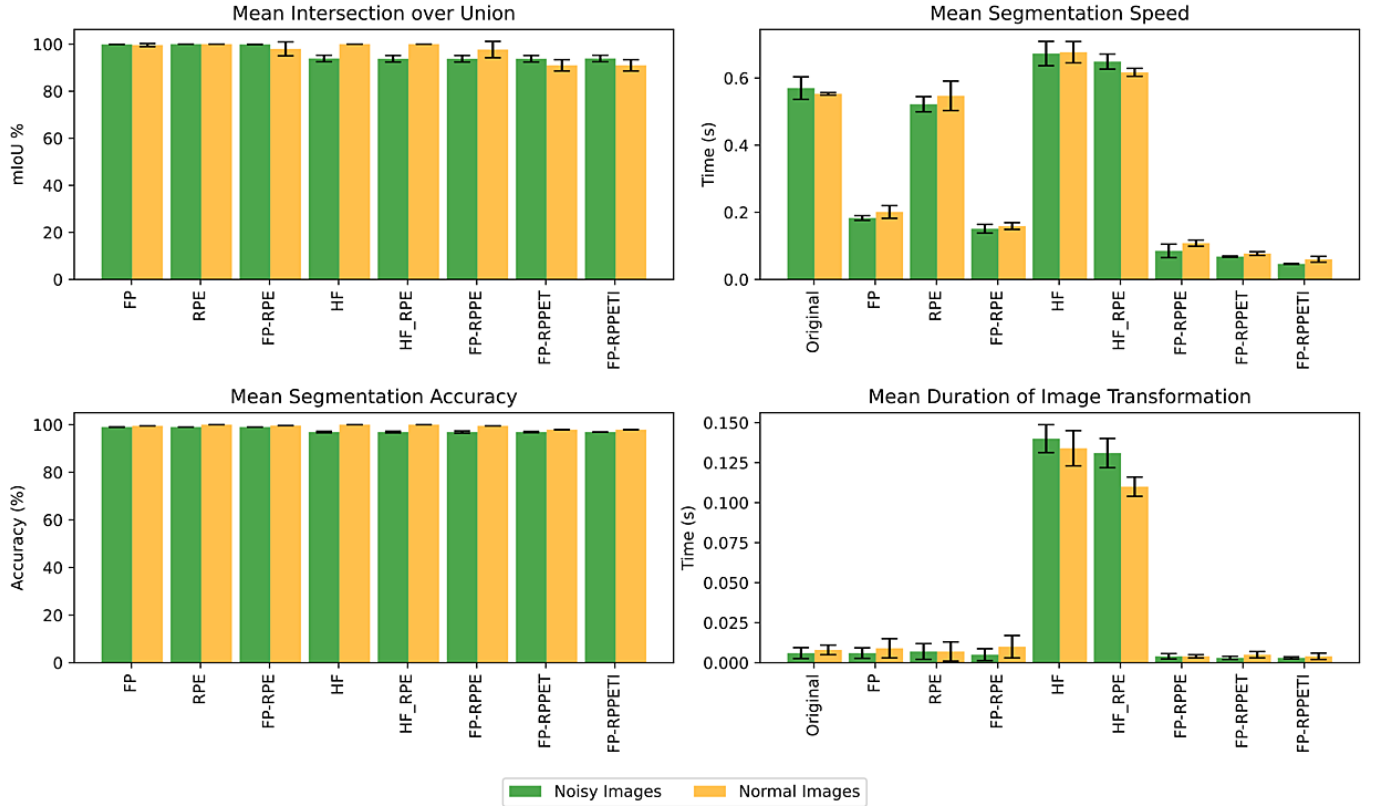


Fig. 8. Comparison of Mean Intersection over Union (mIoU), mean duration of image transformation (seconds), mean segmentation accuracy (the ratio of the correctly segmented area over the ground truth (segmentation of the original CLIPSeg)) and speed between normal and noisy images. Plots for mIoU and mean segmentation accuracy does not include the original CLIPSeg (ground truth).

IV. CONCLUSION

Although the objective of our work was to improve on computational latency, robustness on segmentation is paramount for successful UAV flight operations. By enabling CIoT devices with lightweight VLM aerial segmentation, our efforts reduce the gap of achieving close-to autonomous UAVs. With CIoT devices specifically tailored for AI-Enabled aerial computing, we expect to see more interest in the research of lightweight architectural design for foundation models in UAVs near future. Additionally, there is a need for rigorous tests on hardware deployments of CIoT devices equipped with foundation models to stress-test and validate these models to enable fault-tolerant usage in the setting of UAVs.

V. ACKNOWLEDGEMENT

We would like to highlight the support provided by National Research Council (NRC) Canada for their research guidance and funding, which made our work possible.

REFERENCES

- [1] O. K. Pal, M. S. H. Shovon, M. F. Mridha, and J. Shin, "A Comprehensive Review of AI-enabled Unmanned Aerial Vehicle: Trends, Vision, and Challenges," 2023.
- [2] F. A. Fayaz, A. Malik, and A. A. Yattoo, "Cognitive Internet of Things (CIoT) a Success for Data Collection," in *2021 Sixth International Conference on Image Information Processing (ICIIP)*, vol. 6. IEEE, 2021, pp. 284–287.
- [3] M. Ahn, D. Dwibedi, C. Finn, M. G. Arenas, K. Gopalakrishnan, K. Hausman *et al.*, "AutoRT: Embodied Foundation Models for Large Scale Orchestration of Robotic Agents," 2024.
- [4] J. Huang, S. Yong, X. Ma, X. Linghu, P. Li, Y. Wang *et al.*, "An Embodied Generalist Agent in 3D World," *arXiv preprint arXiv:2311.12871*, 2023.
- [5] F. Liu, D. Chen, Z. Guan, X. Zhou, J. Zhu, and J. Zhou, "RemoteCLIP: A Vision Language Foundation Model for Remote Sensing," 2023.
- [6] H. M. Bong, R. Zhang, R. de Azambuja, and G. Beltrame, "PEACE: Prompt Engineering Automation for CLIPSeg Enhancement in Aerial Robotics," *ArXiv*, 2023.
- [7] K. Rana, J. Haviland, S. Garg, J. Abou-Chakra, I. Reid, and N. Sunderhauf, "SayPlan: Grounding Large Language Models using 3D Scene Graphs for Scalable Task Planning," in *7th Annual Conference on Robot Learning*, 2023.
- [8] Z. Kira, "Awesome-LLM-Robotics," 2022.
- [9] J. Achiam, S. Adler, S. Agarwal, L. Ahmad, I. Akkaya, F. L. Aleman *et al.*, "GPT-4 Technical Report," 2023.
- [10] A. Radford, J. W. Kim, C. Hallacy, A. Ramesh, G. Goh, S. Agarwal *et al.*, "Learning Transferable Visual Models from Natural Language Supervision," 2021.
- [11] H. Touvron, T. Lavril, G. Izacard, X. Martinet, M.-A. Lachaux, T. Lacroix *et al.*, "LLaMA: Open and Efficient Foundation Language Models," 2023.
- [12] W. Niu, X. Ma, S. Lin, S. Wang, X. Qian, X. Lin *et al.*, "PatDNN: Achieving Real-Time DNN Execution on Mobile Devices with Pattern-based Weight Pruning," in *Proceedings of the Twenty-Fifth International Conference on Architectural Support for Programming Languages and Operating Systems*, ser. ASPLOS '20. ACM, Mar. 2020.
- [13] J. Wu, C. Leng, Y. Wang, Q. Hu, and J. Cheng, "Quantized Convolutional Neural Networks for Mobile Devices," 2016.
- [14] Z. Hu, N. Ye, and I. Mohamed, "mmSampler: Efficient Frame Sampler for Multimodal Video Retrieval," in *Proceedings of Machine Learning and Systems*, D. Marculescu, Y. Chi, and C. Wu, Eds., vol. 4, 2022, pp. 153–171.

- [15] M. Yuan, L. Zhang, F. He, X. Tong, M.-H. Song, Z. Xu *et al.*, “InFi: End-to-End Learning to Filter Input for Resource-Efficiency in Mobile-Centric Inference,” 2023.
- [16] U. Drolia, K. Guo, J. Tan, R. Gandhi, and P. Narasimhan, “Towards Edge-Caching for Image Recognition,” in *2017 IEEE International Conference on Pervasive Computing and Communications Workshops, PerCom Workshops 2017, Kona, Big Island, HI, USA, March 13-17, 2017*. IEEE, 2017, pp. 593–598.
- [17] M. Xu, M. Zhu, Y. Liu, F. X. Lin, and X. Liu, “DeepCache: Principled Cache for Mobile Deep Vision,” in *Proceedings of the 24th Annual International Conference on Mobile Computing and Networking*, ser. *MobiCom '18*. ACM, Oct. 2018.
- [18] Q. Cao, P. Khanna, N. D. Lane, and A. Balasubramanian, “MobiVQA: Efficient On-Device Visual Question Answering,” *Proc. ACM Interact. Mob. Wearable Ubiquitous Technol.*, vol. 6, no. 2, jul 2022.
- [19] I. Leontiadis, S. Laskaridis, S. I. Venieris, and N. D. Lane, “It’s always personal: Using Early Exits for Efficient On-Device CNN Personalisation,” in *Proceedings of the 22nd International Workshop on Mobile Computing Systems and Applications*, ser. *HotMobile '21*. ACM, Feb. 2021.
- [20] B. Yang, L. He, N. Ling, Z. Yan, G. Xing, X. Shuai *et al.*, “EdgeFM: Leveraging Foundation Model for Open-Set Learning on the Edge,” 2023.
- [21] M. team, “MLC-LLM,” 2023, accessed: 2024-09-15.
- [22] Y. Wang, K. Chen, H. Tan, and K. Guo, “Tabi: An Efficient Multi-Level Inference System for Large Language Models,” in *Proceedings of the Eighteenth European Conference on Computer Systems*, ser. *EuroSys '23*. New York, NY, USA: Association for Computing Machinery, 2023, p. 233–248.
- [23] L. Chen, M. Zaharia, and J. Zou, “FrugalGPT: How to Use Large Language Models While Reducing Cost and Improving Performance,” 2023.
- [24] X. Sun, P. Zhang, P. Zhang, H. Shah, K. Saenko, and X. Xia, “DIME-FM: Distilling Multimodal and Efficient Foundation Models,” 2023.
- [25] Y. Wei, H. Hu, Z. Xie, Z. Zhang, Y. Cao, J. Bao *et al.*, “Contrastive Learning Rivals Masked Image Modeling in Fine-tuning via Feature Distillation,” 2022.
- [26] W. Dai, L. Hou, L. Shang, X. Jiang, Q. Liu, and P. Fung, “Enabling Multimodal Generation on CLIP via Vision-Language Knowledge Distillation,” 2022.
- [27] C. Zhang, D. Han, Y. Qiao, J. U. Kim, S.-H. Bae, S. Lee *et al.*, “Faster Segment Anything: Towards Lightweight SAM for Mobile Applications,” 2023.
- [28] T. Lüddecke and A. Ecker, “Image Segmentation Using Text and Image Prompts,” in *Proceedings of the IEEE/CVF Conference on Computer Vision and Pattern Recognition (CVPR)*, June 2022, pp. 7086–7096.
- [29] H. M. Bong, R. Zhang, R. de Azambuja, and G. Beltrame, “Dynamic Open Vocabulary Enhanced Safe-landing with Intelligence (DOVESEI),” 2023.
- [30] Y. Li, L. Zhang, and L. Shao, “LR Aerial Photo Categorization by Cross-Resolution Perceptual Knowledge Propagation,” *IEEE Transactions on Neural Networks and Learning Systems*, pp. 1–12, 2024.
- [31] M. K. Mittal, A. Valada, and W. Burgard, “Vision-based Autonomous Landing in Catastrophe-Struck Environments,” *ArXiv*, vol. abs/1809.05700, 2018.
- [32] E. Chatzikalymnios and K. Moustakas, “Landing Site Detection for Autonomous Rotor Wing UAVs Using visual and Structural Information,” *Journal of Intelligent & Robotic Systems*, vol. 104, 02 2022.
- [33] C. Forster, M. Faessler, F. Fontana, M. Werlberger, and D. Scaramuzza, “Continuous On-board Monocular-Vision-based Elevation Mapping Applied to Autonomous Landing of Micro Aerial Vehicles,” in *2015 IEEE International Conference on Robotics and Automation (ICRA)*, 2015, pp. 111–118.
- [34] M. Rabah, A. Rohan, M. Talha, K.-H. Nam, and S. Kim, “Autonomous Vision-based Target Detection and Safe Landing for UAV,” *International Journal of Control, Automation and Systems*, 10 2018.
- [35] J. Park, Y. Kim, and S. Kim, “Landing Site Searching and Selection Algorithm Development Using Vision System and its Application to Quadrotor,” *IEEE Transactions on Control Systems Technology*, vol. 23, no. 2, pp. 488–503, 2015.
- [36] Google, “Google Maps,” accessed: 2023-08-19.
- [37] NVIDIA, “NVIDIA Jetson for Next-Generation Robotics website,” 2024, <https://www.nvidia.com/en-us/autonomous-machines/embedded-systems/>, Last accessed on 2024-09-15.
- [38] E. Perez, F. Strub, H. de Vries, V. Dumoulin, and A. Courville, “FiLM: Visual Reasoning with a General Conditioning Layer,” 2017.
- [39] E. Upton, “Introducing: Raspberry Pi 5!” 2023, <https://www.raspberrypi.com/news/introducing-raspberry-pi-5/>, Last accessed on 2024-09-15.
- [40] D. Thomas, W. Woodall, and E. Fernandez, “Next-generation ROS: Building on DDS,” in *ROSCon Chicago 2014*. Mountain View, CA: Open Robotics, sep 2014.



Haechan Mark Bong (Student Member, IEEE) received his BSc. and MSc. from McGill University, Montréal, QC., Canada, in Computer Science (2018) and Animal Science (2022), respectively. He is currently pursuing his Ph.D. in robotics in Computer and Software Engineering Department in Polytechnique Montréal, QC., Canada, specializing in the application of Vision-Language models in robotics. His research interests are in robotics, LLMs, VLMs, MLLMs, CIoT devices and UAVs.



Ricardo de Azambuja (Member, IEEE) received his B.Sc. (2006) and M.Sc. (2013) degrees in Electrical Engineering from the Federal University of Rio Grande do Sul (UFRGS), Porto Alegre, Brazil, and the Ph.D. degree in Computer Science (Spiking Neural Networks for Humanoid Robot Control) from the University of Plymouth, UK, in 2017. His research journey has spanned diverse areas, including wireless powered sensors, bio-inspired spiking neural networks, collaborative robotics, computer vision, and collision-resilient drones. Currently, he works as a Senior Automation Engineer at Questat.ca, where he is contributing to revolutionizing the biotech blood gases sensor sector.



Giovanni Beltrame (Senior Member, IEEE) received the Ph.D. degree in computer engineering from Politecnico di Milano, Milan, Italy, in 2006. He worked as a Microelectronics Engineer with the European Space Agency, Paris, France, on a number of projects, spanning from radiation tolerant systems to computer-aided design. Since 2010, he has been the Professor with the Computer and Software Engineering Department, Polytechnique Montréal, Montréal, QC., Canada, where he directs the MIST Lab. He has authored or coauthored more than 100 papers in international journals and conferences. His research interests include modeling and design of embedded systems, artificial intelligence, and robotics. Dr. Beltrame was the recipient of more than 30 grants by government agencies and industry.